Turk Neurosurg 36(4):587-607, 2026
DOI: 10.5137/1019-5149.JTN.50630-26.5

Original Investigation
General Neurosurgery and Miscellaneous-Others

Received: 02.12.2025
Accepted: 12.06.2026
Published Online: 24.07.2026

Diffusion Tensor Imaging Metrics Reveal Pronounced Hemispheric Asymmetry in Major White Matter Tracts

Taghi KHANIYEV[1], Efecan CEKIC[2], Muhammed Yakup ALTUG[2], Egemen GOK[2], Sema Nur KIBRIT[2], Bayazit KAYAOGLU[2], Merve PINAR[2], Sahin HANALIOGLU[2,3]

[1]Bilkent University, Faculty of Engineering, Department of Industrial Engineering, Ankara, Türkiye
[2]Hacettepe University, Faculty of Medicine, Department of Neurosurgery, Ankara, Türkiye
[3]Harvard University, Harvard Medical School, Brigham and Women's Hospital, Department of Neurosurgery, Boston, Massachusetts, USA

Corresponding author: Sahin HANALIOGLU ✉ hanalioglu@hacettepe.edu.tr, sahinhanalioglu@gmail.com

ABSTRACT

AIM: To determine hemispheric asymmetries in major white matter tracts using diffusion tensor imaging (DTI) metrics and morphometric measurements, as comprehensive multitract analyses remain limited.

MATERIAL and METHODS: Diffusion MRI data from 102 healthy adults enrolled in the Human Connectome Project (HCP) were analyzed using DSI Studio to reconstruct 17 major white- matter tracts bilaterally. For each tract, diffusion metrics (fractional anisotropy [FA], mean diffusivity [MD], radial diffusivity [RD], axial diffusivity [AD], quantitative anisotropy [QA], isotropic value [ISO], restricted diffusion imaging [RDI], and normalized RDI [nrdı]) and morphometric parameters (fiber count, mean length, trunk volume, branch volume, total volume, and termination region areas) were quantified. Paired t-tests compared left-right hemispheric differences. Multiple comparison corrections were performed with the Benjamini–Krieger–Yekutieli procedure, and effect sizes were reported as Cohen's d.

RESULTS: Significant hemispheric asymmetries were observed in most tracts. FA was significantly higher in the left hemisphere ($p<0.001$) for the arcuate fasciculus (AF), inferior fronto-occipital fasciculus (IFOF), inferior longitudinal fasciculus (ILF), and uncinate fasciculus (UF). Mean diffusivity (MD) demonstrated left dominance in the UF and SLF2-3 ($p=0.009$). QA was predominantly left-lateralized across multiple tracts, including AF, IFOF, ILF, and frontal aslant tract (FAT) ($p<0.01$, Cohen's d: 0.42 to 1.17), except for the vertical occipital fasciculus (VOF), where rightward dominance was noted (Cohen's d: −0.55). Tract-trunk-branch volumes were predominantly left-lateralized in frontal lobe pathways such as AF, SLF1, SLF2, FAT, and UF ($p<0.01$). Rightward dominance was observed in SLF3, parietal aslant tract (PAT), IFOF, ILF, and middle longitudinal fasciculus (MLF) ($p<0.05$). Similar asymmetries were observed in termination region areas, fiber counts, and fiber lengths ($p<0.001$).

CONCLUSION: Widespread hemispheric asymmetries were observed across multiple pathways. Such asymmetry may reflect distinct hemispheric functional specialization and the neurological basis of lateralized functions.

KEYWORDS: DTI, Metrics, Morphometric measurements, Functional topography

Taghi KHANIYEV : 0000-0002-2160-0553
Efecan CEKIC : 0000-0003-2203-5944
Muhammed Yakup ALTUG : 0000-0002-1835-6799
Egemen GOK : 0009-0008-0976-5903
Sema Nur KIBRIT : 0009-0005-2485-6393
Bayazit KAYAOGLU : 0000-0002-9008-2083
Merve PINAR : 0000-0003-3041-6958
Sahin HANALIOGLU : 0000-0003-4988-4938

INTRODUCTION

Diffusion tensor imaging (DTI) and tractography have emerged as indispensable tools in neuroscience and clinical neuroimaging, enabling the non-invasive, in vivo characterization of white matter tracts in the human brain (2,32,33,69). These techniques provide quantitative measures of the geometric, morphometric, and microstructural properties of fiber tracts, enhancing our understanding of the brain's structural connectivity in both healthy individuals and those with neurological disorders, including neurosurgical diseases such as brain tumors, while complementing emerging diagnostic neuroimaging techniques (6,36,39,41,46,50,70).

Previous studies have demonstrated hemispheric asymmetries in specific white matter tracts. Notably, structural lateralization of the arcuate fasciculus (AF), which is implicated in language processing, and the inferior longitudinal fasciculus (ILF), which contributes to visual integration, has been well documented (10,51). Similarly, lateralization has also been observed in subdivisions of the superior longitudinal fasciculus (SLF), which connects the frontal and parietal cortices (16,45). However, most previous studies have examined only a limited number of tracts or relied on a narrow set of DTI metrics. To date, few studies have comprehensively examined tract asymmetries across a wide array of measurements, including fiber count, fiber length, trunk and branch volumes, termination region areas, and diffusion metrics, including fractional anisotropy (FA), mean diffusivity (MD), radial diffusivity (RD), axial diffusivity (AD), quantitative anisotropy (QA), isotropic value (ISO), restricted diffusion imaging (RDI), and normalized RDI (nRDI).

Beyond its theoretical importance, hemispheric asymmetry also has significant clinical relevance. In neurosurgical practice, knowledge of lateralized white matter anatomy can inform resection strategies and facilitate the preservation of neurological function (17,18,31,34). Identifying hemisphere-specific structural differences in white matter tracts can help predict potential postoperative deficits in functions such as language, motor control, and vision. However, such predictions require a systematic and multidimensional evaluation of white matter anatomy.

To address this need, we analyzed 17 major white matter pathways using DTI-based tractography. By examining bilateral microstructural diffusion metrics and macrostructural morphometric measures, we aimed to elucidate the extent and patterns of hemispheric asymmetry in the healthy human brain. The findings may serve as a reference for neuroscience research and clinical applications in neurosurgery, neurology, and neurorehabilitation.

MATERIAL and METHODS

Participants and Data Source

This study analyzed diffusion MRI and handedness data from 102 healthy adults in the Human Connectome Project S2000 database (22). Participants were randomly selected from the publicly available dataset to ensure population-level representativeness. Handedness was assessed using the Edinburgh Handedness Inventory (EHI) (48). As specified in the HCP dataset, hand dominance was determined using a Laterality Quotient (LQ) threshold of ±40%, with positive values indicating right-handedness and negative values denoting left-handedness. Individuals with LQ values equal to ±40 or falling between −40 and +40 were categorized as ambidextrous.

Diffusion MRI Acquisition and Tractography

Diffusion MRI data were acquired at a 3T Siemens Connectom Skyra scanner using the standard HCP multishell diffusion protocol, with b-values of 990, 1985, and 2980 s/mm^2 and 90 sampling directions per shell. The preprocessed HCP diffusion data, aligned to the MNI space, were resampled to 1 -mm isotropic resolution.

Seventeen major white matter pathways were bilaterally reconstructed in each participant's brain using DSI Studio (https://dsi-studio.labsolver.org/), a dedicated diffusion imaging analysis platform. The reconstructed tracts included the AF; frontal, frontoparietal, parietal, parolfactory, and parahippocampal segments of the cingulum; capsula extrema; frontal aslant tract (FAT); inferior fronto-occipital fasciculus (IFOF); ILF; middle longitudinal fasciculus (MLF); parietal aslant tract (PAT); SLF 1, 2, and 3; uncinate fasciculus (UF); and vertical occipital fasciculus (VOF). Anatomical termination regions and functional roles of each tract are summarized in Table I.

Diffusion Reconstruction and Tracking Parameters

Diffusion data were reconstructed using generalized q-sampling imaging with a diffusion sampling length ratio of 1.7 (67). RDI was additionally computed within the DSI Studio processing pipeline. The b-table orientation was confirmed through DSI Studio's automated quality control procedure.

Tract generation for individual bundles was conducted using tract templates provided by DSI Studio. Deterministic fiber tracking was subsequently performed using 1,000,000 seed points. To reduce false-positive streamlines, a topology-informed pruning algorithm was applied iteratively for 16 cycles. Tracking was conducted with an anisotropy threshold of 0.063922, while the angular threshold was randomly varied between 15° and 90°. Step size was randomly selected between 0.5 and 1.5 voxels, and streamline length was constrained to a range of 30–300 mm. For atlas-based tract mapping, a distance tolerance of 16 mm was applied. Regions of avoidance were defined at coordinates 75, 96, 62 with a total volume of 1.6 × 106 mm^3.

Measurement Parameters

For each white matter tract, bilateral morphometric and microstructural measurements were obtained. Morphometric parameters included fiber count, mean fiber length, trunk volume, branch volume, total tract volume, and areas of termination regions. Furthermore, multiple DTI-derived microstructural metrics were evaluated, including FA, MD, RD, AD, QA, ISO, RDI, and nrdı. The clinical implications and interpretations of these DTI metrics are presented in Table II.

Statistical Analysis

Statistical analyses were performed using graphpad Prism version 8.4.2. The Shapiro–Wilk and Kolmogorov–Smirnov tests

Table I: Cortical Endpoints and Functional Roles of Study-Included White Matter Tracts

Tract	Origin	Termination	Funcitonal Role
Arcuate Fasciculus (AF)	Posterior superior temporal gyrus	Inferior frontal gyrus	Dorsal language pathway; phonological processing (10)
Cingulum – Frontal	Medial prefrontal cortex	Anterior cingulate cortex	Executive functions, emotional regulation (7,40,62)
Cingulum – Frontoparietal	ACC/dorsal cingulate	Posterior cingulate/ precuneus	Default mode network connectivity (7,40,62)
Cingulum – Parietal	Posterior cingulate	Angular gyrus	Episodic memory and visuospatial integration (7,40,62)
Cingulum – Parolfactory	Medial orbitofrontal cortex	Paraterminal gyrus	Limbic–prefrontal communication (7,40,62)
Cingulum – Parahippocampal	Posterior cingulate	Parahippocampal gyrus	Memory encoding and retrieval (7,40,62)
Capsula Extrema	Superior temporal gyrus	Inferior frontal gyrus	Ventral semantic language pathway (45)
Frontal Aslant Tract (FAT)	SMA / pre-SMA	Inferior frontal gyrus	Speech initiation, volitional control (44)
Inferior Front-Occipital Fasciculus (IFOF)	Occipital cortex	Inferior frontal gyrus/OFC	Semantic processing, visual–language integration (14)
Inferior Longitudinal Fasciculus (ILF)	Occipital pole	Anterior temporal lobe	Object recognition, face processing (35)
Middle Longitudinal Fasciculus (MLF)	Superior temporal gyrus	Inferior parietal lobule	Auditory–parietal semantic pathway (19)
Parietal Aslant Tract (PAT)	Inferior parietal lobule	angular gyrus/posterior temporal lobe	Pragmatic language, working memory integration (49)
SLF-I	Superior parietal lobule	Medial premotor cortex/SMA	Motor planning and spatial attention (59)
SLF-II	Supramarginal/Angular gyrus	Dorsolateral prefrontal cortex	Working memory, attentional control (38,59)
SLF-III	Supramarginal gyrus	Inferior frontal gyrus	Phonological processing and articulation (39)
Uncinate Fasciculus (UF)	Temporal pole/Amygdala	Orbitofrontal cortex	Semantic memory, social–emotional evaluation (60)
Vertical Occipital Fasciculus (VOF)	Lateral occipital cortex	Fusiform/ITG	Reading, dorsal–ventral visual integration (48)

were used to assess data normality. Paired two-tailed t-tests were performed for evaluating left-right hemispheric differences across all metrics. A p value of <0.05 was considered statistically significant. Statistical correction for multiple comparisons was applied using the false discovery rate two-stage step-up procedure of Benjamini, Krieger, and Yekutieli, with a q value of <0.01 considered statistically significant. Effect sizes were quantified using Cohen's d for each tract and parameter.

RESULTS

Results were analyzed in two separate categories: DTI metrics and morphometric results. Among the 102 participants included in the study, 87 were right-handed (85.3%), 2 were left-handed (2.0%), and 13 were ambidextrous (12.7%). Since most participants were right-handed, additional statistical analyses of both DTI metrics and morphometric measurements were conducted within the right-handed subgroup to mitigate the potential confounding effect of handedness on hemispheric asymmetry.

Diffusion Tensor Imaging Metrics

Analysis of diffusion metrics revealed significant hemispheric asymmetries across multiple tracts. FA was significantly higher in the left hemisphere in the arcuate fasciculus (AF) ($p<0.0001$, $d=1.43$), inferior fronto-occipital fasciculus ($p<0.0001$, $d=0.71$), inferior longitudinal fasciculus ($p<0.0001$, $d=0.72$), and frontal aslant tract ($p<0.0001$, $d=0.82$). Conversely, rightward FA asymmetry was observed in SLF2 ($p<0.01$, $d=–0.50$) and SLF3 ($p<0.0001$, $d=–0.75$).

Table II: DTI Metrics and Clinical Implications of Study-Included White Matter Tracts

Metric	Clinical implication	Interpretation
Fractional anisotropy (FA)	FA is nonspecifically associated with axonal integrity	decreases: demyelination, inflammation, edema, axonal loss (13)
Axial diffusivity (AD)	AD is interpreted as a marker of axonal integrity	decreases: axonal loss (8,54)
Radial diffusivity (RD)	RD is nonspecifically associated with myelination	increases: demyelination (8,55,56)
Mean diffusivity (MD)	MD is associated with edema and cell infiltration	increases: vesogenic edema, decreases: cytotoxic edema (55,56)
Quantitative diffusivity (QA)	QA is associated with axonal density	decreases: axonal loss (53,68)
Isotrpic value (ISO)	ISO is associated with edema	increases: edema (68)
Restricte diffusion imaging (RDI)	RDI is associated with cellular infiltration related to inflammation or tumor presence.	increases: cell infiltrations (inflammation or tumor infiltration) (16,65)
Normalized RDI	NRDI is associated with edema	increases: edema due to inflammation (66)

MD demonstrated rightward dominance in the AF ($p<0.0001$, $d=–0.61$), frontoparietal cingulum ($p<0.0001$, $d=–1.25$), frontal–parahippocampal cingulum ($p<0.01$, $d=–0.37$), and parolfactory cingulum ($p<0.0001$, $d=–1.53$), whereas leftward MD dominance was observed in SLF2 ($p<0.001$, $d=0.50$), SLF3 ($p<0.001$, $d=0.51$), IFOF ($p<0.01$, $d=0.43$), and uncinate fasciculus ($p<0.0001$, $d=0.69$).

RD exhibited rightward dominance in the AF ($p<0.0001$, $d=–0.90$), frontoparietal cingulum ($p<0.0001$, $d=–2.04$), frontal–parahippocampal cingulum ($p<0.0001$, $d=–0.60$), parolfactory cingulum ($p<0.0001$, $d=–0.73$), and IFOF ($p<0.001$, $d=–0.49$). In contrast, SLF2 ($p<0.0001$, $d=0.60$) and SLF3 ($p<0.001$, $d=0.54$) exhibited leftward RD asymmetry.

QA was predominantly left lateralized, with significant asymmetry in the AF ($p<0.01$, $d=0.44$), FAT ($p<0.0001$, $d=0.83$), IFOF ($p<0.001$, $d=0.54$), ILF ($p<0.01$, $d=0.42$), frontal–parahippocampal cingulum ($p<0.0001$, $d=0.56$), and frontoparietal cingulum ($p<0.0001$, $d=1.17$). The vertical occipital fasciculus showed rightward QA asymmetry ($p<0.001$, $d=–0.55$).

AD showed leftward asymmetry in the FAT ($p<0.0001$, $d=0.60$), ILF ($p<0.0001$, $d=0.86$), and SLF1 ($p<0.0001$, $d=0.57$). Rightward AD asymmetry was noted in the PAT ($p<0.0001$, $d=–1.10$), parolfactory cingulum ($p<0.0001$, $d=–1.26$), and VOF ($p<0.0001$, $d=–0.84$).

ISO was significantly greater in the left hemisphere in the FAT ($p<0.0001$, $d=0.57$) and parolfactory cingulum ($p<0.001$, $d=0.49$), whereas the VOF exhibited rightward ISO dominance ($p<0.001$, $d=–0.47$).

RDI and normalized RDI2L (nrdı2l) values demonstrated leftward asymmetry in the parolfactory cingulum (RDI: $p<0.001$, $d=0.52$; nrdı2l: $p<0.01$, $d=0.52$) and FAT (RDI: $p<0.0001$, $d=0.62$; nrdı2l: $p<0.0001$, $d=0.59$), whereas rightward dominance was observed in the VOF (RDI: $p<0.001$, $d=–0.50$; nrdı2l: $p<0.001$, $d=–0.50$). Notably, increasing the normalized RDI level (nrdı-L) from 02 to 04 revealed additional rightward asymmetry in the PAT ($p<0.01$, $d=–0.45$), indicating that greater q-space sensitivity may detect additional hemispheric lateralization patterns.

All statistically significant DTI metric results are detailed in Table III and summarized in Table IV. Additionally, the significant tract data are illustrated in Figure 1 using color-coded visualizations. Mean AD, FA, MD, and RD values for six tracts (FAT, IFOF, AF, UF, SLF2, and ILF) in both hemispheres, along with their hemispheric asymmetry graphs and statistical significance levels, are displayed in Figure 2.

Morphometric Results

Morphometric analysis revealed consistent hemispheric asymmetries across major white matter tracts. Leftward dominance was observed in the AF, FAT, ILF, SLF1, SLF2, and UF for most morphometric measures.

The FAT exhibited leftward asymmetry in all parameters except for fiber count, where no significant difference was observed. Significant leftward asymmetry in the AF was also noted across all morphometric parameters except for mean length, which exhibited rightward dominance ($p<0.0001$, $d=–1.05$).

SLF1 and SLF2 demonstrated left-sided dominance, whereas SLF3 displayed rightward asymmetry in all morphometric parameters. The IFOF exhibited rightward asymmetry across most morphometric features. Exceptions included mean length ($p<0.0001$, $d=1.49$), which was greater in the left hemisphere, and trunk volume, which did not differ significantly between hemispheres.

The parahippocampal and parolfactory segments of the cingulum were predominantly left lateralized, whereas the frontoparietal and parietal-parahippocampal segments were right-dominant. The extreme capsule exhibited significant rightward asymmetry in the second end -region area ($p<0.0001$, $d=–0.70$), total end-region area ($p<0.01$, $d=–0.39$), and mean length ($p<0.01$, $d=–0.43$).

The PAT demonstrated rightward asymmetry across most parameters with no significant laterality in irregularity, mean length, and branch volume. The VOF exhibited leftward asymmetry only in irregularity ($p<0.0001$, $d=0.63$) and total surface

Table III: Results of Diffusion Tensor and Advanced Diffusion Metrics Across Major White Matter Tracts. This table presents mean diffusion parameters for the left and right hemispheres, including axial diffusivity (AD), fractional anisotropy (FA), isotropic value (ISO), mean diffusivity (MD), radial diffusivity (RD), quantitative anisotropy (QA), restricted diffusion imaging (RDI), and normalized RDI (nRDI2L, nRDI4L). Differences (L–R), standard errors, dominant hemispheres, and corresponding Cohen's d values are shown for each tract.

Tract	p-value	Left	Right	Difference (L–R)	SE of difference	Dominant side	Cohen's d value
Axial diffusivity (AD)							
Cingulum Parolfactory	**< 0.0001**	0.7603	0.8046	–0.0443	0.004934	Right	-1.26
Frontal Aslant Tract	**< 0.0001**	0.7871	0.7704	+0.0167	0.003864	Left	0.60
Inferior Longitudinal Fasciculus	**< 0.0001**	0.8447	0.8172	+0.0275	0.004494	Left	0.86
Parietal Aslant Tract	**< 0.0001**	0.8289	0.8632	–0.0343	0.004367	Right	-1.10
Superior Longitudinal Fasciculus1	**< 0.0001**	0.7775	0.7648	+0.0127	0.003132	Left	0.57
VOF (Vertical Occipital Fasciculus)	**< 0.0001**	0.7958	0.8201	–0.0243	0.004027	Right	-0.84
Fractional anisotrophy (FA)							
Arcuate Fasciculus	**< 0.0001**	0.4185	0.3874	+0.03116	0.003052	Left	1.43
Cingulum Frontal Parahippocampal	**< 0.0001**	0.3958	0.3749	+0.02086	0.003969	Left	0.74
Cingulum Frontal Parietal	**< 0.0001**	0.4088	0.3532	+0.05561	0.003428	Left	2.27
Frontal Aslant Tract	**< 0.0001**	0.3616	0.3453	+0.01631	0.002782	Left	0.82
IFOF (Inferior Fronto Occipital)	**< 0.0001**	0.4154	0.4006	+0.01479	0.002911	Left	0.71
ILF (Inferior Long. Fasc.)	**< 0.0001**	0.3941	0.3787	+0.01542	0.003005	Left	0.72
Middle Longitudinal Fasc.	**< 0.001**	0.3465	0.3584	–0.01186	0.003322	Right	-0.50
Parietal Aslant Tract	**< 0.0001**	0.3965	0.3820	+0.01448	0.002947	Left	0.69
SLF2	**< 0.001**	0.3878	0.3987	–0.01089	0.003034	Right	-0.50
SLF3	**< 0.0001**	0.3750	0.3928	–0.01772	0.003326	Right	-0.75
Isotropic value (ISO)							
Cingulum Parolfactory	**< 0.001**	0.3170	0.2972	+0.01985	0.005663	Left	0.49
Frontal Aslant Tract	**< 0.0001**	0.3667	0.3375	+0.02916	0.007142	Left	0.57
VOF (Vertical Occipal Fasciculus)	**< 0.001**	0.4583	0.4914	–0.03312	0.009801	Right	-0.47
Mean diffusivity (MD)							
Arcuate Fasciculus	**< 0.0001**	0.5305	0.5399	–0.009385	0.002140	Right	-0.61
Cingulum Frontal Parahippocampal	**< 0.01**	0.5341	0.5415	–0.007448	0.002796	Right	-0.37
Cingulum Frontal Parietal	**< 0.0001**	0.5311	0.5545	–0.02342	0.002615	Right	-1.25
Cingulum Parolfactory	**< 0.0001**	0.5376	0.5717	–0.03413	0.003116	Right	-1.53
IFOF	**< 0.01**	0.5510	0.5429	+0.008101	0.002623	Left	0.43
ILF	**< 0.001**	0.5555	0.5652	–0.009634	0.002687	Right	-0.50
MLF (Middle Long. Fasc.)	**< 0.01**	0.5760	0.5689	+0.007146	0.002519	Left	0.40
Parietal Aslant Tract	**< 0.0001**	0.5596	0.5698	–0.01021	0.002543	Right	-0.56
SLF2	**< 0.001**	0.5499	0.5418	+0.008116	0.002295	Left	0.50
SLF3	**< 0.001**	0.5625	0.5526	+0.009950	0.002721	Left	0.51
Uncinate Fasciculus	**< 0.0001**	0.5713	0.5567	+0.01465	0.002977	Left	0.69
VOF (Vertical Occipital Fasciculus)	**< 0.001**	0.5483	0.5576	–0.009281	0.002514	Right	-0.52

Table III: Cont.

Tract	p-value	Left	Right	Difference (L–R)	SE of difference	Dominant side	Cohen's d value
Normalized restricted diffusion imaging 02L (nRDI2L)							
Cingulum Parolfactory	**< 0.01**	0.2674	0.2512	+0.01614	0.004373	Left	0.52
Frontal Aslant Tract	**< 0.0001**	0.3089	0.2842	+0.02475	0.005850	Left	0.59
VOF (Vertical Occipital Fasciculus)	**< 0.001**	0.3933	0.4247	-0.03148	0.008806	Right	-0.50
Normalized restricted diffusion imaging 04L (nRDI4L)							
Cingulum Parolfactory	**< 0.00001**	0.03870	0.03512	+0.003583	0.0007244	Left	0.69
Frontal Aslant Tract	**< 0.00001**	0.04272	0.03884	+0.003881	0.0008179	Left	0.66
Parietal Aslant Tract	**< 0.01**	0.04360	0.04657	-0.002965	0.0009239	Right	-0.45
VOF (Vertical Occipital Fasciculus)	**< 0.001**	0.05599	0.06068	-0.004687	0.001257	Right	-0.52
Quantitative anisotrophy (QA)							
Arcuate Fasciculus	**< 0.01**	0.2322	0.2178	+0.01441	0.004543	Left	0.44
Cingulum Frontal Parahippocampal	**< 0.0001**	0.2053	0.1887	+0.01661	0.004164	Left	0.56
Cingulum Frontal Parietal	**< 0.0001**	0.2136	0.1793	+0.03434	0.004121	Left	1.17
Frontal Aslant Tract	**< 0.0001**	0.2153	0.1893	+0.02600	0.004387	Left	0.83
IFOF	**< 0.001**	0.2480	0.2295	+0.01851	0.004774	Left	0.54
ILF	**< 0.01**	0.2376	0.2228	+0.01481	0.004889	Left	0.42
VOF (Vertical Occipital Fasciculus)	**< 0.001**	0.2591	0.2836	–0.02448	0.006255	Right	-0.55
Radial diffusivity (RD)							
Arcuate Fasciculus	**< 0.0001**	0.4060	0.4230	–0.01698	0.002632	Right	-0.90
Cingulum Frontal Parahippocampal	**< 0.0001**	0.4124	0.4264	–0.01401	0.003243	Right	-0.60
Cingulum Frontal Parietal	**< 0.0001**	0.4092	0.4555	–0.04636	0.003189	Right	-2.04
Cingulum Parolfactory	**< 0.0001**	0.4536	0.4717	–0.01810	0.003463	Right	-0.73
IFOF (Inferior Fronto Occipital Fasc.)	**< 0.001**	0.4264	0.4372	–0.01074	0.003093	Right	-0.49
Parietal Aslant Tract	**< 0.0001**	0.4386	0.4676	–0.02904	0.002881	Right	-1.41
SLF2	**< 0.0001**	0.4308	0.4199	+0.01090	0.002547	Left	0.60
SLF3	**< 0.001**	0.4495	0.4369	+0.01254	0.003230	Left	0.54
VOF	**< 0.0001**	0.4411	0.4557	–0.01465	0.002993	Right	-0.69
Restricted Diffusion Imaging (RDI)							
Cingulum Parolfactory	**< 0.001**	0.4059	0.3773	+0.02857	0.007671	Left	0.52
Frontal Aslant Tract	**< 0.0001**	0.4699	0.4323	+0.03766	0.008467	Left	0.62
VOF (Vertical Occipital Fasciculus)	**< 0.001**	0.5811	0.6281	-0.04697	0.01320	Right	-0.50

area ($p<0.0001$, $d=0.60$), with no significant differences in other morphometric parameters.

All statistically significant morphometric parameter results are presented in Table V and summarized in Table VI. Additionally, the significant tract data are illustrated in Figure 3 employing color-coded visualizations. Figure 4 presents a schematic illustration of the morphometric workflow, including their graphical representation and 3D brain projection for the AF and IFOF, encompassing the number of tracts, end regions, and branch volume. Figure 5 schematically depicts Cohen's d effect sizes derived from the measurements of all DTI metrics and morphometric parameters included in the study.

Table IV: Summary of Hemispheric Dominance for Diffusion Metrics Across Major White Matter Tracts. This table summarizes the lateralization patterns (Left [L], Right [R], or non-significant [-]) observed for each diffusion metric, including axial diffusivity (AD), fractional anisotropy (FA), isotropic value (ISO), mean diffusivity (MD), quantitative anisotropy (QA), radial diffusivity (RD), restricted diffusion imaging (RDI), and normalized RDI values (nRDI2L and nRDI4L).

Tract	AD	FA	ISO	MD	QA	RD	RDI	nRDI2L	nRDI4L
Arcuate Fasciculus	-	L	-	R	L	R	-	-	-
Cingulum Frontal Parahippocampal	-	L	-	R	L	R	-	-	-
Cingulum Frontal Parietal	-	L	-	R	L	R	-	-	-
Cingulum Parahippocampal	-	-	-	-	-	-	-	-	-
Cingulum Parahippocampal Parietal	-	-	-	-	-	-	-	-	-
Cingulum Parolfactory	R	-	L	R	-	R	L	L	L
Extreme Capsule	-	-	-	-	-	-	-	-	-
Frontal Aslant Tract	L	L	L	-	L	-	L	L	L
Inferior Fronto Occipital Fasciculus (IFOF)	-	L	-	L	L	R	-	-	-
Inferior Longitudinal Fasciculus (ILF)	L	L	-	R	L	-	-	-	-
Middle Longitudinal Fasciculus (MLF)	-	R	-	L	-	-	-	-	-
Parietal Aslant Tract	R	L	-	R	-	R	-	-	R
Superior Longitudinal Fasciculus1 (SLF1)	L	-	-	-	-	-	-	-	-
Superior Longitudinal Fasciculus2 (SLF2)	-	R	-	L	-	L	-	-	-
Superior Longitudinal Fasciculus3 (SLF3)	-	R	-	L	-	L	-	-	-
Uncinate Fasciculus (UF)	-	-	-	L	-	-	-	-	-
Vertical Occipital Tract (VOF)	R	-	R	R	R	R	R	R	R

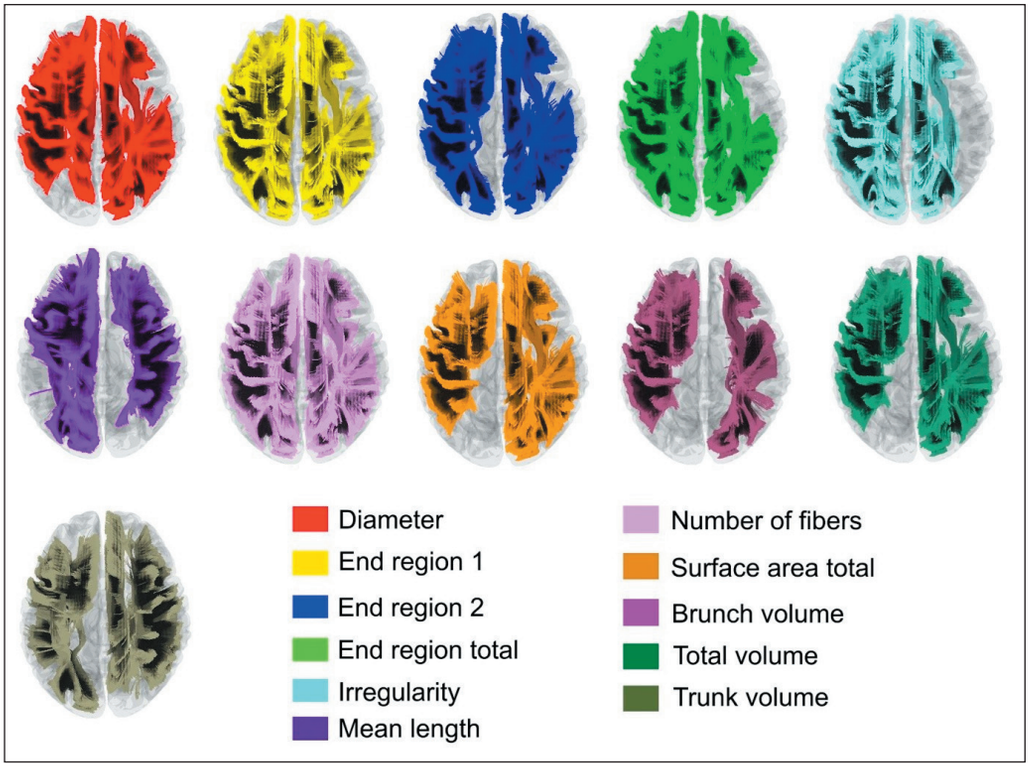

Figure 1: Color-coded representation of white matter tracts depicting statistically significant hemispheric asymmetry based on diffusion tensor imaging metrics. Each tract is displayed on the hemisphere, demonstrating dominant expression of the corresponding DTI parameter.

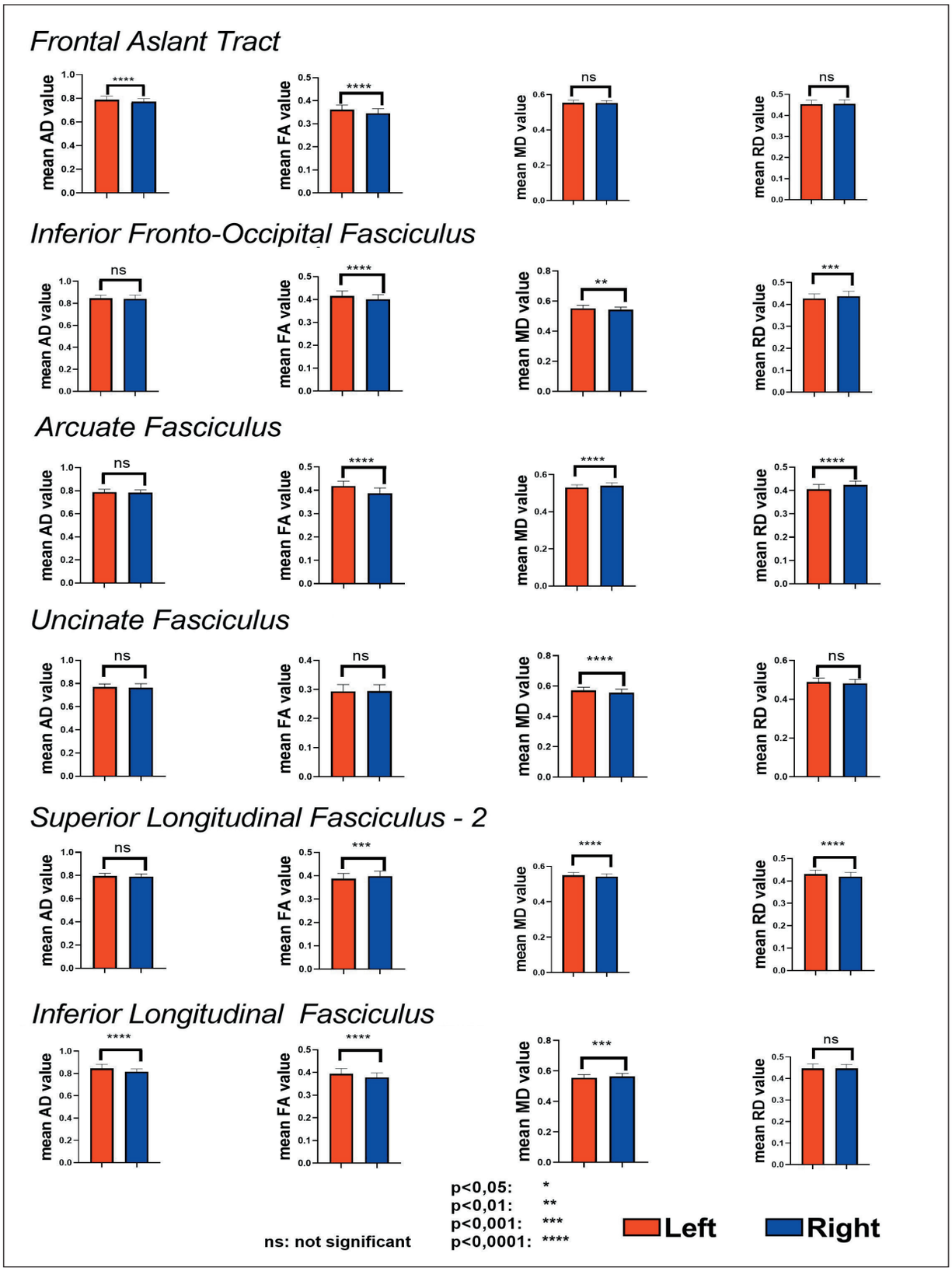

Figure 2: Graphical representation of the mean AD, FA, MD, and RD values for six white- matter tracts (frontal aslant tract, inferior fronto-occipital fasciculus, arcuate fasciculus, uncinate fasciculus, superior longitudinal fasciculus II, and inferior longitudinal fasciculus), along with the statistical significance levels of their hemispheric asymmetries.

Table V: Quantitative Morphometric Measurements of Major White Matter Tracts. This table presents the mean morphometric parameters (diameter, end region areas, irregularity, length, fiber count, surface area, and volume measures) for the left and right hemispheres. Differences (L–R), standard errors, and Cohen's d values are provided for each tract, with the dominant hemisphere indicated.

Tract	p-value	Left	Right	Difference (L–R)	SE of difference	Dominant side	Cohen's d value
			Diameter (mm)				
Arcuate Fasciculus	**< 0.0001**	12.72	7.284	+5.432	0.2948	Left	2.58
Cingulum Parahippocampal	**< 0.0001**	12.12	10.68	+1.447	0.1991	Left	1.02
Cingulum Parolfactory	**< 0.0001**	9.377	7.323	+2.055	0.1361	Left	2.11
Frontal Aslant Tract	**< 0.0001**	16.14	13.61	+2.521	0.2775	Left	1.27
Superior Longitudinal Fasciculus1 (SLF1)	**< 0.0001**	11.11	7.905	+3.207	0.1887	Left	2.38
Superior Longitudinal Fasciculus2 (SLF2)	**< 0.0001**	17.34	12.51	+4.834	0.2855	Left	2.37
Uncinate Fasciculus	**< 0.0001**	12.69	10.77	+1.912	0.1774	Left	1.51
Cingulum Frontal Parietal	**< 0.0001**	9.509	13.55	–4.043	0.1466	Right	-3.86
Cingulum Parahippocampal Parietal	**< 0.0001**	6.940	8.717	–1.777	0.1800	Right	-1.38
Inferior Fronto Occipital Fasciculus (IFOF)	**< 0.0001**	10.10	11.71	–1.611	0.2282	Right	-0.99
Middle Longitudinal Fasciculus (MLF)	**< 0.0001**	5.836	8.583	–2.746	0.2744	Right	-1.40
Parietal Aslant Tract	**< 0.0001**	16.08	19.76	–3.678	0.2680	Right	-1.92
Superior Longitudinal Fasciculus3 (SLF3)	**< 0.0001**	13.84	16.18	–2.342	0.1918	Right	-1.71
			Area of end region - 1st (mm^3)				
Arcuate Fasciculus	**< 0.0001**	1609	569.5	+1040	75.33	Left	1.93
Cingulum Frontal Parahippocampal	**< 0.0001**	365.2	282.6	+82.6	17.97	Left	0.64
Cingulum Parahippocampal	**< 0.0001**	1580	1068	+512.2	54.74	Left	1.31
Cingulum Parolfactory	**< 0.0001**	1414	885.7	+528.5	52.63	Left	1.41
Frontal Aslant Tract	**< 0.0001**	2041	1523	+518.3	92.35	Left	0.79
Inferior Longitudinal Fasciculus (ILF)	**< 0.0001**	2260	1608	+651.8	112.5	Left	0.81
Superior Longitudinal Fasciculus1 (SLF1)	**< 0.0001**	1152	436.5	+715.8	40.37	Left	2.48
Superior Longitudinal Fasciculus2 (SLF2)	**< 0.0001**	1980	1363	+616.8	92.78	Left	0.93
Uncinate Fasciculus	**< 0.01**	1605	1392	+212.7	63.80	Left	0.47
Cingulum Frontal Parietal	**< 0.0001**	995.2	1934	–938.9	58.79	Right	-2.24
Cingulum Parahippocampal Parietal	**< 0.0001**	482.8	964.3	–481.5	47.06	Right	-1.43
Inferior Fronto Occipital Fasciculus (IFOF)	**< 0.0001**	1008	1905	–896.8	78.23	Right	-1.61
Middle Longitudinal Fasciculus (MLF)	**< 0.0001**	231.3	492.9	–261.6	34.79	Right	-1.05
Parietal Aslant Tract	**< 0.0001**	2708	4120	–1412	144.0	Right	-1.37
Superior Longitudinal Fasciculus3 (SLF3)	**< 0.0001**	1427	1940	–512.7	68.01	Right	-1.06
			Area of end region – 2nd (mm^3)				
Arcuate Fasciculus	**< 0.0001**	1605	553.8	+1051	73.81	Left	1.99
Cingulum Parolfactory	**< 0.0001**	998.1	656.5	+341.6	31.10	Left	1.54
Frontal Aslant Tract	**< 0.0001**	2266	1556	+710.1	93.37	Left	1.06
Inferior Longitudinal Fasciculus (ILF)	**< 0.0001**	1841	1198	+643.6	84.13	Left	1.07
Superior Longitudinal Fasciculus1 (SLF1)	**< 0.0001**	1014	389.2	+625.1	37.59	Left	2.33
Superior Longitudinal Fasciculus2 (SLF2)	**< 0.0001**	2399	1258	+1141	94.78	Left	1.69

Table V: Cont.

Tract	p-value	Left	Right	Difference (L–R)	SE of difference	Dominant side	Cohen's d value
Uncinate Fasciculus	**< 0.0001**	1371	878.1	+492.8	63.40	Left	1.09
Cingulum Frontal Parietal	**< 0.0001**	1097	2664	–1567	63.39	Right	-3.46
Cingulum Parahippocampal Parietal	**< 0.0001**	271.4	416.7	–145.4	23.35	Right	-0.87
Extreme Capsule	**< 0.0001**	329.6	551.4	–221.9	44.34	Right	-0.70
Inferior Fronto Occipital Fasciculus (IFOF)	**< 0.01**	1398	1692	–294.8	92.08	Right	-0.45
Middle Longitudinal Fasciculus (MLF)	**< 0.0001**	347.7	906.7	–559.0	59.88	Right	-1.31
Parietal Aslant Tract	**< 0.0001**	2067	3080	–1013	103.9	Right	-1.36
Superior Longitudinal Fasciculus3 (SLF3)	**< 0.0001**	1477	2329	–852.3	70.76	Right	-1.69
			Area of end region – total (mm³)				
Arcuate Fasciculus	**< 0.0001**	3214	1123	+2090	143.3	Left	2.04
Cingulum Frontal Parietal	**< 0.0001**	2092	4598	–2505	111.6	Right	-3.14
Cingulum Parahippocampal	**< 0.0001**	2405	1859	+546.4	88.76	Left	0.86
Cingulum Parahippocampal Parietal	**< 0.0001**	754.2	1381	–626.9	64.06	Right	-1.37
Cingulum Parolfactory	**< 0.0001**	2412	1542	+870.1	72.61	Left	1.68
Extreme Capsule	**< 0.01**	761.1	1015	–254.3	92.29	Right	-0.39
Frontal Aslant Tract	**< 0.0001**	4307	3078	+1228	174.8	Left	0.98
Inferior Fronto Occipital Fasciculus (IFOF)	**< 0.0001**	2405	3597	–1192	159.8	Right	-1.04
Inferior Longitudinal Fasciculus (ILF)	**< 0.0001**	4101	2806	+1295	187.2	Left	0.97
Middle Longitudinal Fasciculus (MLF)	**< 0.0001**	579.0	1400	–820.6	91.16	Right	-1.26
Parietal Aslant Tract	**< 0.0001**	4775	7200	–2424	233.8	Right	-1.45
Superior Longitudinal Fasciculus1 (SLF1)	**< 0.0001**	2167	825.6	+1341	72.63	Left	2.59
Superior Longitudinal Fasciculus2 (SLF2)	**< 0.0001**	4379	2621	+1758	180.6	Left	1.36
Superior Longitudinal Fasciculus3 (SLF3)	**< 0.0001**	2904	4269	–1365	129.4	Right	-1.48
Uncinate Fasciculus	**< 0.0001**	2976	2270	+705.4	111.1	Left	0.89
				Irregularity			
Arcuate Fasciculus	**< 0.0001**	9.435	7.124	+2.312	0.1660	Left	1.95
Cingulum Frontal Parietal	**< 0.0001**	7.831	9.548	–1.717	0.08410	Right	-2.86
Cingulum Parahippocampal	**< 0.0001**	8.921	8.152	+0.7686	0.09134	Left	1.18
Cingulum Parahippocampal Parietal	**< 0.0001**	6.463	7.317	–0.8538	0.09538	Right	-1.25
Cingulum Parolfactory	**< 0.0001**	7.362	6.222	+1.140	0.09303	Left	1.72
Frontal Aslant Tract	**< 0.0001**	9.789	9.307	+0.4823	0.09076	Left	0.74
Inferior Fronto Occipital Fasciculus (IFOF)	**< 0.0001**	8.427	9.123	–0.6960	0.1075	Right	-0.91
Inferior Longitudinal Fasciculus (ILF)	**< 0.001**	10.92	11.34	–0.4250	0.1170	Right	-0.51
Superior Longitudinal Fasciculus1 (SLF1)	**< 0.001**	8.904	8.144	+0.7594	0.2217	Left	0.48
Superior Longitudinal Fasciculus2 (SLF2)	**< 0.0001**	12.44	10.54	+1.904	0.2323	Left	1.15
Superior Longitudinal Fasciculus3 (SLF3)	**< 0.0001**	9.929	10.99	–1.059	0.1116	Right	-1.33
Uncinate Fasciculus	**< 0.0001**	8.968	7.184	+1.784	0.1038	Left	2.41
Vertical Occipital Fasciculus (VOF)	**< 0.0001**	9.414	8.820	+0.5943	0.1318	Left	0.63

Table V: Cont.

Tract	p-value	Left	Right	Difference (L–R)	SE of difference	Dominant side	Cohen's d value
			Mean lenght (mm)				
Arcuate Fasciculus	**< 0.0001**	120.9	130.4	–9.508	1.272	Right	-1.05
Cingulum Parolfactory	**< 0.0001**	75.97	118.0	–41.98	1.233	Right	-4.77
Extreme Capsule	**< 0.01**	93.06	96.32	–3.263	1.051	Right	-0.43
Superior Longitudinal Fasciculus2	**< 0.0001**	68.12	96.61	–28.49	1.444	Right	-2.76
Superior Longitudinal Fasciculus3	**< 0.0001**	61.32	70.95	–9.633	1.034	Right	-1.30
Uncinate Fasciculus	**< 0.0001**	70.52	74.67	–4.149	1.044	Right	-0.56
Cingulum Frontal Parahippocampal	**< 0.01**	115.3	110.6	+4.711	1.570	Left	0.42
Cingulum Frontal Parietal	**< 0.0001**	108.6	99.10	+9.530	1.384	Left	0.96
Cingulum Parahippocampal	**< 0.0001**	47.16	44.47	+2.690	0.4263	Left	0.88
Cingulum Parahippocampal Parietal	**< 0.0001**	96.51	90.39	+6.119	1.109	Left	0.77
Frontal Aslant Tract	**< 0.0001**	79.42	76.48	+2.946	0.5391	Left	0.77
Inferior Fronto Occipital Fasciculus (IFOF)	**< 0.0001**	174.0	162.2	+11.78	1.105	Left	1.49
Inferior Longitudinal Fasciculus (ILF)	**< 0.01**	114.2	111.5	+2.718	0.9309	Left	0.41
Middle Longitudinal Fasciculus (MLF)	**< 0.0001**	108.6	91.29	+17.31	1.546	Left	1.57
			Number of fibers				
Arcuate Fasciculus	**< 0.0001**	36649	15581	+21068	2290	Left	1.29
Cingulum Frontal Parahippocampal	**< 0.001**	17287	12604	+4682	1289	Left	0.51
Cingulum Parolfactory	**< 0.0001**	94122	41694	+52428	3119	Left	2.35
Inferior Longitudinal Fasciculus (ILF)	**< 0.0001**	48886	26110	+22776	2626	Left	1.21
Superior Longitudinal Fasciculus1 (SLF1)	**< 0.0001**	26135	6794	+19341	1116	Left	2.43
Superior Longitudinal Fasciculus2 (SLF2)	**< 0.0001**	38310	22479	+15832	2093	Left	1.06
Cingulum Frontal Parietal	**< 0.0001**	31100	59366	–28266	2184	Right	-1.81
Cingulum Parahippocampal Parietal	**< 0.0001**	16550	24995	–8446	1958	Right	-0.60
Inferior Fronto Occipital Fasciculus (IFOF)	**< 0.0001**	25763	40216	–14454	2313	Right	-0.87
Middle Longitudinal Fasciculus (MLF)	**< 0.0001**	7836	27625	–19790	2314	Right	-1.20
Parietal Aslant Tract	**< 0.0001**	71595	101522	–29926	4856	Right	-0.86
Superior Longitudinal Fasciculus3 (SLF3)	**< 0.0001**	42916	54937	–12021	2634	Right	-0.64
Uncinate Fasciculus	**< 0.0001**	67505	84464	–16959	3854	Right	-0.62
			Total surface area (mm^3)				
Arcuate Fasciculus	**< 0.0001**	45999	21685	+24314	1343	Left	2.53
Cingulum Frontal Parietal	**< 0.0001**	25608	40283	–14674	731.5	Right	-2.81
Cingulum Parahippocampal	**< 0.0001**	16132	12244	+3888	388.6	Left	1.40
Cingulum Parahippocampal Parietal	**< 0.0001**	13706	18215	–4509	500.8	Right	-1.26
Frontal Aslant Tract	**< 0.0001**	39517	30523	+8994	846.8	Left	1.49
Inferior Fronto Occipital Fasciculus (IFOF)	**< 0.0001**	47033	54678	–7645	1455	Right	-0.74
Middle Longitudinal Fasciculus (MLF)	**< 0.0001**	14783	18966	–4183	887.4	Right	-0.66
Parietal Aslant Tract	**< 0.0001**	36625	45280	–8655	844.8	Right	-1.43
Superior Longitudinal Fasciculus1 (SLF1)	**< 0.0001**	23347	15685	+7662	666.8	Left	1.61

Table V: Cont.

Tract	p-value	Left	Right	Difference (L–R)	SE of difference	Dominant side	Cohen's d value
Superior Longitudinal Fasciculus2 (SLF2)	**< 0.001**	46166	40856	+5310	1586	Left	0.47
Superior Longitudinal Fasciculus3 (SLF3)	**< 0.0001**	26434	39629	–13195	715.4	Right	-2.58
Uncinate Fasciculus	**< 0.0001**	25346	18401	+6944	655.5	Left	1.48
Vertical Occipital Fasciculus (VOF)	**< 0.0001**	22211	20025	+2185	506.3	Left	0.60
				Branch volume (mm³)			
Arcuate Fasciculus	**< 0.0001**	7769	2806	+4964	333.4	Left	2.08
Cingulum Parahippocampal Parietal	**< 0.0001**	1627	2136	–509	124.9	Right	-0.57
Frontal Aslant Tract	**< 0.001**	2258	1526	+732.2	208.9	Left	0.49
Inferior Fronto Occipital Fasciculus (IFOF)	**< 0.0001**	7974	9941	–1967	454.7	Right	-0.61
Inferior Longitudinal Fasciculus (ILF)	**< 0.001**	10472	12360	–1889	521.4	Right	-0.51
Middle Longitudinal Fasciculus (MLF)	**< 0.01**	1423	1888	–465.2	142.7	Right	-0.46
Superior Longitudinal Fasciculus1 (SLF1)	**< 0.001**	2514	1924	+589.9	167.8	Left	0.49
Superior Longitudinal Fasciculus2 (SLF2)	**< 0.0001**	10262	7597	+2665	501.1	Left	0.74
Superior Longitudinal Fasciculus3 (SLF3)	**< 0.0001**	3744	5859	–2115	307.1	Right	-0.96
Uncinate Fasciculus	**< 0.0001**	4809	2755	+2054	204.2	Left	1.41
				Trunk volume (mm³)			
Arcuate Fasciculus	**< 0.0001**	7858	3112	+4746	464.8	Left	1.43
Cingulum Frontal Parietal	**< 0.0001**	3012	9046	–6034	371.2	Right	-2.28
Cingulum Parahippocampal	**< 0.0001**	4335	3062	+1273	204.5	Left	0.87
Cingulum Parahippocampal Parietal	**< 0.0001**	2167	3372	–1204	202.2	Right	-0.83
Frontal Aslant Tract	**< 0.0001**	14252	9796	+4456	601.6	Left	1.04
Inferior Longitudinal Fasciculus (ILF)	**< 0.0001**	6443	3593	+2850	439.8	Left	0.91
Middle Longitudinal Fasciculus (MLF)	**< 0.0001**	1839	3769	–1931	285.2	Right	-0.95
Parietal Aslant Tract	**< 0.0001**	10425	16751	–6326	700.6	Right	-1.26
Superior Longitudinal Fasciculus1 (SLF1)	**< 0.0001**	4841	1959	+2882	249.8	Left	1.62
Superior Longitudinal Fasciculus3 (SLF3)	**<0.0001**	5601	8822	–3222	438.9	Right	-1.03
				Total volume (mm³)			
Arcuate Fasciculus	**< 0.0001**	15628	5918	+9710	543.1	Left	1.43
Cingulum Frontal Parietal	**< 0.0001**	7854	14352	–6498	304.2	Right	-2.28
Cingulum Parahippocampal	**< 0.0001**	5555	4047	+1507	179.8	Left	0.87
Cingulum Parahippocampal Parietal	**< 0.0001**	3794	5507	–1713	203.8	Right	-0.83
Frontal Aslant Tract	**< 0.0001**	16511	11322	+5188	508.3	Left	1.04
Inferior Fronto Occipital Fasciculus (IFOF)	**< 0.0001**	14432	17673	–3241	625.6	Right	-0.33
Middle Longitudinal Fasciculus (MLF)	**< 0.0001**	3262	5658	–2396	315.0	Right	-0.95
Parietal Aslant Tract	**< 0.0001**	13712	20168	–6456	489.1	Right	-1.26
Superior Longitudinal Fasciculus1 (SLF1)	**< 0.0001**	7356	3884	+3472	216.5	Left	1.62
Superior Longitudinal Fasciculus2 (SLF2)	**< 0.0001**	16212	12466	+3746	629.8	Left	0.33
Superior Longitudinal Fasciculus3 (SLF3)	**< 0.0001**	9345	14682	–5337	349.7	Right	-1.03
Uncinate Fasciculus	**< 0.0001**	9028	6935	+2094	279.9	Left	0.02

Table VI: Summary of Morphometric Lateralization Patterns Across Major White Matter Tracts. This table summarizes the dominant hemisphere (Left [L] or Right [R]) for each morphometric parameter, as detailed in Table IV.

Tract	Diam.	EndR1	EndR2	EndR Total	Irreg.	Mean Length	N. of Fibers	Surf. Area Total	Vol. Brunch	Vol. Total	Vol. Trunk
AF	L	L	L	L	L	R	L	L	L	L	L
CFPH	-	L	-	-	-	L	L	-	-	-	-
CFP	R	R	R	R	R	L	R	R	-	R	R
CPH	L	L	-	L	L	L	-	L	-	L	L
CPHP	R	R	R	R	R	L	R	R	R	R	R
CP	L	-	L	L	L	R	L	-	-	-	-
EC	-	-	R	R	-	R	-	-	-	-	-
FAT	L	L	L	L	L	L	-	L	L	L	L
IFOF	R	R	R	R	R	L	R	R	R	R	-
ILF	-	L	L	L	R	L	L	-	R	-	L
MLF	R	R	R	-	-	L	R	R	R	R	R
PAT	R	R	R	R	-	-	R	R	-	R	R
SLF1	L	L	L	L	L	-	L	L	L	L	L
SLF2	L	L	L	L	L	R	L	L	L	L	-
SLF3	R	R	R	R	R	R	R	R	R	R	R
UF	L	L	L	L	L	R	R	L	L	L	-
VOF	-	-	-	-	L	-	-	L	-	-	-

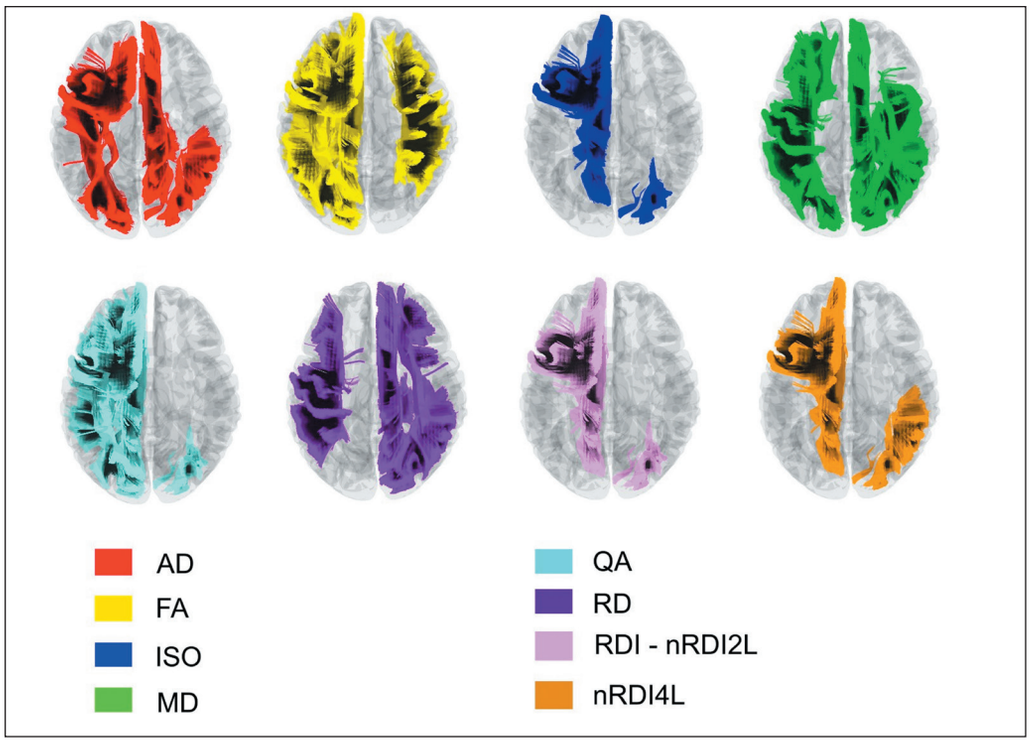

Figure 3: Color-coded representation of white matter tracts demonstrating statistically significant hemispheric asymmetry based on morphometric measurements. Each tract is displayed on the hemisphere where the corresponding morphometric parameter is dominant.

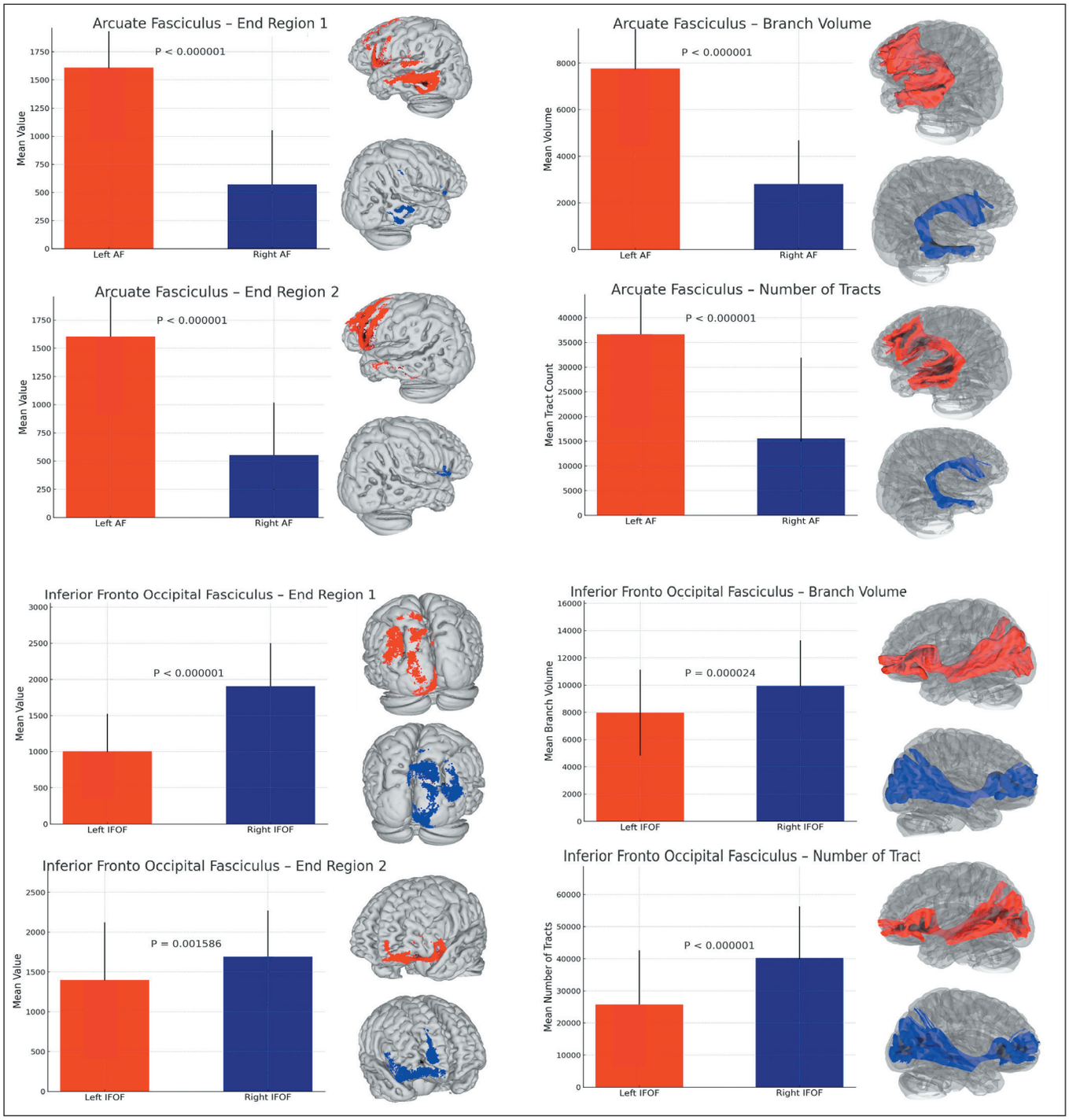

Figure 4: Graphical representation of the mean number of tracts, end-region distributions, and branch volumes of the arcuate fasciculus and inferior fronto-occipital fasciculus, together with their corresponding representations projected onto a three-dimensional brain model.

Right-Handed Subgroup Analysis

All statistical analyses were repeated in the right-handed subgroup to assess robustness and to control for potential confounding by handedness. The results were consistent with those of the full cohort. Subgroup analysis revealed no statistically significant deviations or newly emerging effects. The direction and magnitude of hemispheric asymmetries in both DTI metrics and morphometric measures remained consistent.

In the AF, leftward asymmetry was noted for FA, number of tracts, and total volume, whereas MD, RD, and mean length demonstrated rightward asymmetry (each $p<0.0001$). Within SLF2, FA was right lateralized, whereas MD and RD demonstrated leftward asymmetry. Mean length exhibited rightward asymmetry, whereas the number of tracts and total volume demonstrated leftward asymmetry (mean length, number of tracts, and volume: $p<0.0001$; FA, MD, and RD: $p<0.01$). No significant asymmetry was detected in SLF1 for FA or MD; however, tract volume, number of tracts, and AD were left-lateralized (each $p<0.0001$). In SLF3, FA exhibited rightward asymmetry ($p<0.0001$), while MD and RD showed leftward asymmetry ($p<0.01$); additionally, mean length, number of tracts, and total volume demonstrated rightward dominance (all $p<0.0001$).

Within the cingulum, FA demonstrated leftward asymmetry in the frontal–parahippocampal segment ($p<0.0001$), while the frontal–parietal segment exhibited rightward asymmetry ($p<0.0001$). RD was right-lateralized in both the frontal–parietal and frontal–parahippocampal segments (each $p<0.0001$). Mean length demonstrated leftward asymmetry across all cingulum segments except the parolfactory subdivision (each $p<0.01$). Regarding the number of tracts, leftward dominance was recorded in the parolfactory and frontal–parahippocampal segments, whereas rightward dominance was detected in the frontal–parietal and parietal-parahippocampal segments (each $p<0.001$).

DISCUSSION

This study systematically examined hemispheric asymmetries in major white matter tracts by combining DTI metrics with morphometric measurements (Figure 5). Our results indicate that lateralization varies across tracts or modalities, showing highly tract-specific and metric-specific patterns rather than a uniform organization. Language-related tracts, including the AF, FAT, ILF, and UF, demonstrated pronounced leftward asymmetry across multiple microstructural indices (FA, MD, and QA) and morphometric parameters (tract volume and termination area). However, the rightward asymmetry observed in the MD of the AF represents an exception to this overall pattern. These findings are consistent with established left-hemisphere dominance for language processing and provide further insight into the structural basis for this functional lateralization (10,21). In contrast, tracts such as SLF2, SLF3, PAT, and VOF demonstrated rightward asymmetry, particularly in FA, RD, and morphometric measures, consistent with their roles in attentional, motor, and visuospatial processing. The IFOF showed rightward asymmetry in morphometric indices but not consistently in diffusion metrics, suggesting that lateralization may be primarily macrostructural without corresponding microstructural differences.

Our findings align with previous studies reporting leftward asymmetry in language-related tracts and rightward asymmetry in attentional and visuospatial pathways (49,56). Nevertheless, structural lateralization of the AF, particularly in monolingual individuals, has been linked to language abilities, including vocabulary and semantic fluency (1,62). In one study, AF fiber counts demonstrated leftward asymmetry in both right- and left-handed individuals, while FA remained symmetrical (1). No association between right-handedness and AF lateralization was identified. The authors further reported that the streamline lateralization of the AF correlated with language performance, whereas FA lateralization did not; however, these findings did not remain significant after correction for multiple comparisons (1). Unlike our findings, a previous study reported lower MD values in the right AF compared with the left AF irrespective of handedness, with no significant differences in total volume or mean fiber length (64). In our study, however, MD values were lower on the left, mean fiber length was greater on the right, and both total volume and trunk volume were left-lateralized. Notably, this study included trilingual participants, and the authors reported a correlation between fmrı-determined language lateralization and DTI findings in monolingual individuals. The observed discrepancy between the two studies may therefore be related to the random selection of participants in our cohort, independent of the number of languages spoken.

Furthermore, some studies report increased fiber density in the AF independent of handedness or functional language lateralization, suggesting that structural AF asymmetry may not directly determine hemispheric language dominance (60). However, the authors reported that right-handedness was associated with fmrı language lateralization ($p=0.001$). This discrepancy may reflect differences in the functional connectivity patterns captured by DTI and fmrı methodologies. In this context, one study reported AF-related bilateral language lateralization in 52% of participants using DTI, compared with only 4% in the same cohort using fmrı (64). Overall, these findings indicate a more complex relationship between AF tractographic lateralization and functional connectivity lateralization than previously assumed, with the present study providing a useful reference framework.

The SLF, a key pathway for visuospatial attention, is generally considered symmetric when evaluated as a whole (16). Nevertheless, the right SLF is often reported to have greater volume than the left (38,47). In our study, SLF1 and SLF2 exhibited leftward dominance in total volume, whereas SLF3 was right-dominant. For trunk volume, SLF1 was left-dominant and SLF3 right-dominant, while SLF2 demonstrated no significant asymmetry. Previous studies frequently attribute the apparent overall symmetry of the SLF to the inclusion of SLF1 within the total structure (16,38). Conversely, some studies have reported leftward lateralization of SLF2, which connects frontoparietal and frontotemporal regions (5,57,59,61) and has been linked to language lateralization. Overall, the literature remains inconclusive regarding the lateralization of the SLF and its subcomponents. These inconsistencies underscore the need for further randomized controlled studies with robust datasets to better elucidate structural and functional lateralization and the relationship between them.

In a study of the cingulum, a fiber-based approach rather than an ROI-based analysis revealed significantly higher left hemispheric FA values across all segments except the posterior portion, with no significant association between lateralization

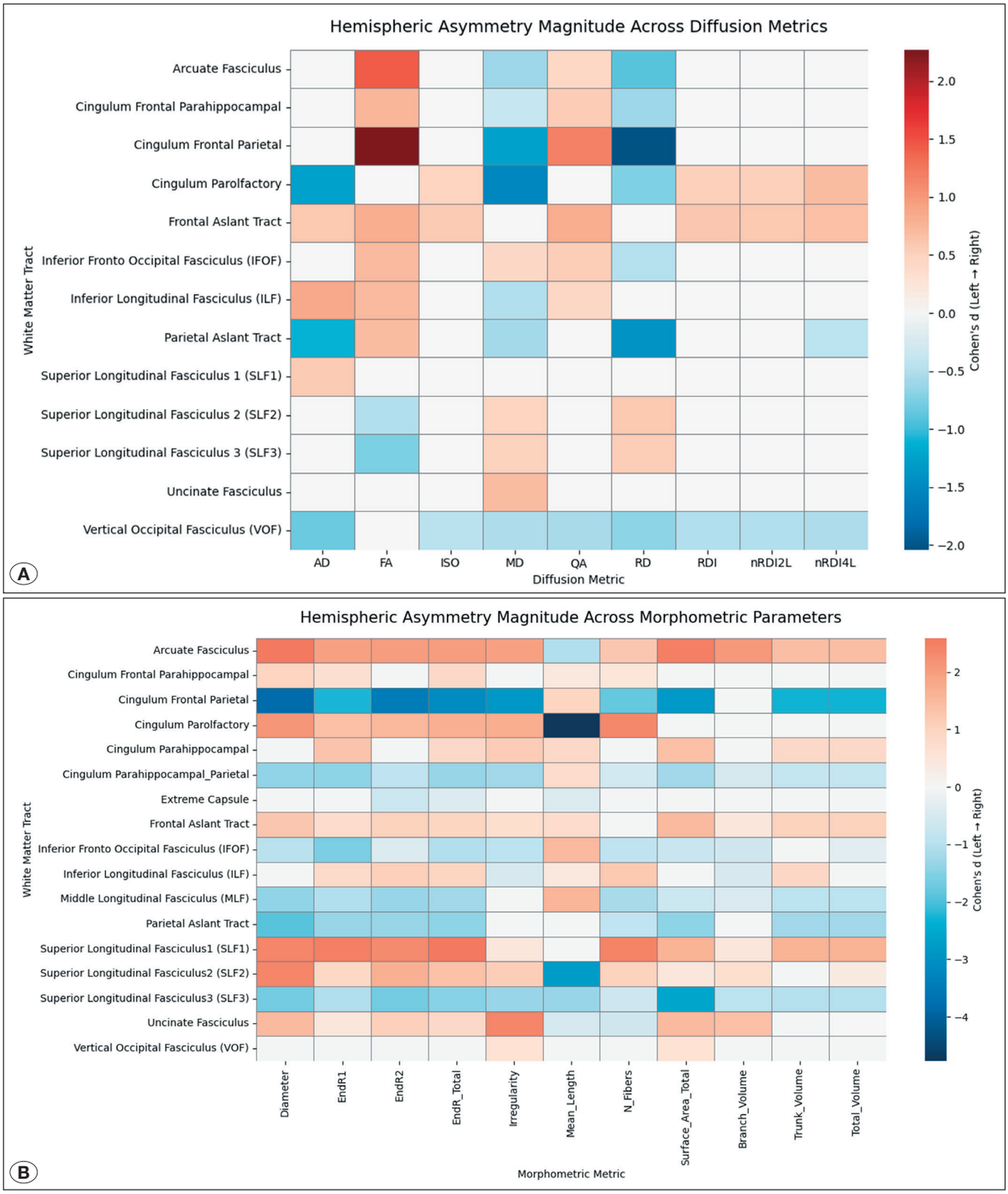

Figure 5: Hemispheric asymmetry heatmaps for diffusion and morphometric metrics. **A)** Heatmap depicting tract-specific hemispheric asymmetries across diffusion measures (FA, MD, AD, RD, QA, ISO, RDI, nrdı2l, and nrdı4l). Positive Cohen's d values (blue tones) denote leftward dominance, whereas negative values (red tones) indicate rightward dominance. **B)** Corresponding heatmap illustrating asymmetry profiles across morphometric parameters (diameter, fiber count, mean length, end-region area, surface area, and tract volumes). Color intensity reflects the magnitude of Cohen's d, representing the strength of lateralization for each tract and metric.

and handedness (23). In that study, bilateral FA elevation was observed only in right-handed individuals, a finding consistent with the results of our study. Similarly, in our cohort, significant leftward FA dominance was observed in the frontoparietal and frontal–parahippocampal segments, with no significant lateralization in the posterior segments. The absence of significant differences between the DTI results of the entire cohort and those of the right-handed subgroup further supports previous evidence that handedness is not consistently associated with the lateralization of DTI findings.

The observed divergences between metrics, such as leftward asymmetry in QA alongside rightward asymmetry in RD within the same tract, indicate that white matter asymmetry is multidimensional and cannot be captured by a single metric. These patterns, evident across both diffusion- and geometry-based analyses, underscore the complexity of hemispheric specialization and emphasize the need for a multimodal approach to evaluate white matter asymmetry. By incorporating additional measures of microstructural and diffusional heterogeneity, such as QA, ISO, and RDI, this study offers a more nuanced perspective on lateralization. The use of RDI and nrdı, in particular, has enabled the detection of fiber density variations that are not readily captured by conventional tensor models. Increased q-space sensitivity in nrdı4l further revealed rightward asymmetry in the PAT, highlighting the sensitivity of higher- order diffusion models (9). These results may help explain cross-modal discrepancies in lateralization and emphasize the importance of high-resolution, multishell acquisition schemes, such as those in the HCP dataset. Moreover, incorporating techniques such as neurite orientation dispersion and density imaging and multi-compartment modeling may better delineate the microstructural asymmetries and their linkage to cortical functions (15,71).

Another key strength of this study lies in its methodological rigor. By using a consistent ROI-based segmentation approach across 17 bilaterally tracked fiber bundles and analyzing diverse metrics under the same pipeline, we minimized variability and maximized comparability across participants and tracts. Moreover, effect sizes were systematically reported alongside significance values to reflect both statistical and practical relevance. The combined assessment of macrostructural and microstructural asymmetries offers a robust basis for future research exploring sex differences, developmental trajectories, or neuropathological alterations in white matter lateralization. In this context, group-wise tractometry pipelines, such as tractseg and bundlewarp, provide scalable tools for delineating variability and asymmetry in large neuroimaging cohorts (52).

Importantly, these asymmetry profiles have substantial clinical relevance, particularly for neurosurgical planning. Tracts such as the AF and FAT, which consistently demonstrated leftward dominance, are frequently located near eloquent cortical regions supporting language production and executive function. Recognizing normative asymmetry in these structures is essential for differentiating physiological lateralization from pathological changes, such as tumor-induced displacement or edema. The use of lateralized morphometric and microstructural profiles may enhance preoperative risk stratification and help inform resection boundaries to minimize postoperative functional deficits. Moreover, the observed dissociation between morphometric and diffusion-based asymmetries in certain tracts (e.g., IFOF and VOF) suggests that reliance on a single modality may yield incomplete or potentially misleading interpretations. Therefore, multimodal tractography protocols incorporating both geometric and diffusion metrics may enhance intraoperative decision-making, especially in patients with lesions in close proximity to high-risk fiber bundles. These normative asymmetry maps may serve as a valuable reference for individualized, function-preserving neurosurgical approaches (3,18,33,49,62). Recent studies emphasize that integrating tractography into neuronavigation systems and 3D models improves the localization of eloquent pathways and surgical safety margins during resection (4,24-28).

Nevertheless, some limitations should be acknowledged. While the study used a relatively large and well-curated dataset, its cross-sectional design limits inference on developmental or age-related changes. Additionally, DTI-based metrics, while informative, are indirect proxies of histological properties and require cautious interpretation, especially when making clinical extrapolations (50,65). Furthermore, hemispheric asymmetries may be influenced by individual differences in handedness, cognitive strategies, or structural anomalies not explicitly controlled for in this dataset. Previous studies have demonstrated that metrics derived from both the whole brain and major white matter tracts may be affected by extrinsic factors. Although studies in children link handedness to the lateralization of functional connectivity, mean DTI metrics also vary by sex and age (53,58). Similar variability has been observed in monozygotic twins, where male twins, concordant twin pairs, and right-handed twins tend to exhibit a leftward predisposition in AF lateralization (30), suggesting nongenetic influences on cerebral network asymmetry. Accordingly, it is increasingly recognized that accounting for individual variability in white matter structure is critical for accurately characterizing lateralization patterns, particularly in clinical populations (20). However, due to the random selection of participants in this study, the number of left-handed and ambidextrous individuals was inadequate for sufficiently powered subgroup analyses. Future studies with larger samples of left-handed and ambidextrous participants are therefore warranted to more definitively clarify the relationship between handedness and white matter lateralization.

Future studies may benefit from integrating large-scale datasets and leveraging machine learning techniques to predict functional lateralization patterns from structural features. Additionally, incorporating three-dimensional tract models into augmented and virtual reality-based intraoperative navigation systems could further improve surgical planning and outcomes. Integrating diffusion metrics with AI-assisted diagnostic tools, large clinical datasets, and 3D segmentations may enable the development of personalized asymmetry maps, thereby improving diagnostic accuracy, treatment, and rehabilitation strategies in both research and clinical neurosurgical settings (11,12,29,37,42,43,63).

CONCLUSION

This study comprehensively evaluated hemispheric asymmetry in major white matter tracts using morphometric and advanced diffusion metrics. The findings confirm distinct lateralization patterns, particularly leftward dominance in language-related tracts and rightward dominance in attentional and visuospatial pathways. These normative asymmetry profiles may inform neurosurgical planning, enhance tract-specific risk assessment, and enable personalized neurorehabilitation. Future work integrating AI, large-scale datasets, and 3D visualization tools may further refine clinical applications of tractography-based asymmetry analysis.

ACKNOWLEDGEMENTS

Preparation for publication of this article is partly supported by Turkish Neurosurgical Society. The authors would like to thank Enago (www.enago.com) for the English language review.

Declarations

Funding: This research did not receive any specific grant from funding agencies in the public, commercial, or not-for-profit sectors.

Availability of data and materials: The datasets used and/or analysed during the current study available from the corresponding author on reasonable request.

Disclosure: The authors have no personal, financial, or institutional interest in any drugs, materials, or devices described in this article.

Ethics approval and consent to participate: The present study used de-identified, publicly available data from the Human Connectome Project (HCP). No new participant recruitment or data collection was performed. Therefore, additional institutional review board approval was not required for this secondary analysis.

AUTHORSHIP CONTRIBUTION

Study conception and design: TK, EC, MYA, SH

Data collection: TK, EC, SNK, BK, MP, SH

Analysis and interpretation of results: TK, EC, MYA, EG, SNK, BK, MP, SH

Draft manuscript preparation: TK, EC, MYA, SH

Critical revision of the article: TK, EC, MYA, EG, SH

Other (study supervision, fundings, materials, etc...): TK, EC, MYA, EG, SNK, BK, MP, SH

All authors (TK, EC, MYA, EG, SNK, BK, MP, SH) reviewed the results and approved the final version of the manuscript.

REFERENCES

1. Allendorfer JB, Hernando KA, Hossain S, Nenert R, Holland SK, Szaflarski JP: Arcuate fasciculus asymmetry has a hand in language function but not handedness. Human Brain Mapping 37:3297-3309, 2016
2. Auriat AM, Borich MR, Snow NJ, Wadden KP, Boyd LA: Comparing a diffusion tensor and non-tensor approach to white matter fiber tractography in chronic stroke. Neuroimage Clin 7:771-781, 2015. https://doi.org/10.1016/j.nicl.2015.03.007
3. Aydin I, Cavusoglu N, Kef B, Gokceli A, Cekic E, Hanalioglu S, Gok E, Asilturk M, Demirgil BT: Association of A1 segment morphology with the rupture risk and morphology of anterior communicating artery aneurysms: a retrospective, single-center study. J Clin Med 15:1376, 2026. https://doi.org/10.3390/jcm15041376
4. Aylmore H, Young F, Aquilina K, Clark CA, Clayden JD: The use of intraoperative tractography in brain tumor and epilepsy surgery: a systematic review and meta-analysis. Front Neuroimaging 4:1563996, 2025. https://doi.org/10.3389/fnimg.2025.1563996
5. Baydin SS, Barut O, Kucukyuruk B, Hasimoglu O, Tanriover N: Anatomical segmentation and connectivity of the uncinate fasciculus. Turk Neurosurg 35:652-660, 2025. https://doi.org/10.5137/1019-5149.JTN.49120-25.2.
6. Brown DA, Hanalioglu S, Chaichana K, Duffau H: Transcorticosubcortical approach for left posterior mediobasal temporal region gliomas: a case series and anatomic review of relevant white matter tracts. World Neurosurg 139:e737-e747, 2020. https://doi.org/10.1016/j.wneu.2020.04.147.
7. Bubb EJ, Metzler-Baddeley C, Aggleton JP: The cingulum bundle: Anatomy, function, and dysfunction. Neurosci Biobehav Rev 92:104-127, 2018. https://doi.org/10.1016/j.neubiorev.2018.05.008
8. Budde MD, Kim JH, Liang HF, Schmidt RE, Russell JH, Cross AH, Song SK: Toward accurate diagnosis of white matter pathology using diffusion tensor imaging. Magn Reson Med 57:688-695, 2007
9. Catani M, Allin MPG, Husain M, Pugliese L, Mesulam MM, Murray RM, Jones DK: Symmetries in human brain language pathways correlate with verbal recall. Proc Natl Acad Sci U S A 104:17163-17168, 2007. https://doi.org/10.1073/pnas.0702116104
10. Catani M, Jones DK, ffytche DH. Perisylvian language networks of the human brain. Ann Neurol 57:8-16, 2005. https://doi.org/10.1002/ana.20319
11. Cekic E, Cetin G, Ozer AG, Baylarov B, Gok E, Tatar I, Hanalioglu S: Digital 3D models in neurosurgical training, surgical planning, and intraoperative guidance: Narrative review of the literature. World Neurosurgery: X 30:100580, 2026. https://doi.org/10.1016/j.wnsx.2026.100580
12. Cekic E, Pinar E, Pinar M, Dagcinar A: Deep learning-assisted segmentation and classification of brain tumor types on magnetic resonance and surgical microscope images. World Neurosurgery 182:e196-e204, 2024. https://doi.org/10.1016/j.wneu.2023.11.073
13. Chang EH, Argyelan M, Aggarwal M, Chandon T-SS, Karlsgodt KH, Mori S, Malhotra AK: The role of myelination in measures of white matter integrity: Combination of diffusion tensor imaging and two-photon microscopy of CLARITY intact brains. Neuroimage 147:253-261, 2017. https://doi.org/10.1016/j.neuroimage.2016.11.068
14. Conner AK, Briggs RG, Sali G, Rahimi M, Baker CM, Burks JD, Glenn CA, Battiste JD, Sughrue ME: A connectomic atlas of the human cerebrum—chapter 13: tractographic description of the inferior fronto-occipital fasciculus. Oper Neurosurg 15:S436-S443, 2018. https://doi.org/10.1093/ons/opy267

15. Daducci A, Canales-Rodríguez EJ, Descoteaux M, Garyfallidis E, Gur Y, Lin YC, Mani M, Merlet S, Paquette M, Ramirez-Manzanares A, Reisert M, Reis Rodrigues P, Sepehrband F, Caruyer E, Choupan J, Deriche R, Jacob M, Menegaz G, Prčkovska V, Rivera M, Wiaux Y, Thiran JP: Quantitative comparison of reconstruction methods for intra-voxel fiber recovery from diffusion MRI. IEEE Trans Med Imaging 33:384-399, 2014. https://doi.org/10.1109/TMI.2013.2285500
16. De Schotten MT, Dell'Acqua F, Forkel SJ, Simmons A, Vergani F, Murphy DGM, Catani M: A lateralized brain network for visuospatial attention. Nat Neurosci 14:1245-1246, 2011. https://doi.org/10.1038/nn.2905
17. Duffau H: A personal consecutive series of surgically treated 51 cases of insular WHO Grade II glioma: advances and limitations. J Neurosurg 110:696-708, 2009. https://doi.org/10.3171/2008.8.JNS08741
18. Duffau H: Stimulation mapping of white matter tracts to study brain functional connectivity. Nat Rev Neurol 11:255-265, 2015. https://doi.org/10.1038/nrneurol.2015.51
19. Fiester P, Baig SA, Patel J, Rao D: An anatomic, imaging, and clinical review of the medial longitudinal fasciculus. J Clin Imaging Sci 10:83, 2020. https://doi.org/10.25259/JCIS_49_2020
20. Forkel SJ, Thiebaut de Schotten M, Kawadler JM, Dell'Acqua F, Danek A, Catani M: The anatomy of fronto-occipital connections from early blunt dissections to contemporary tractography. Cortex 56:73-84, 2014. https://doi.org/10.1016/j.cortex.2012.09.005
21. Geschwind N, Levitsky W: Human brain: left-right asymmetries in temporal speech region. Science 161:186-187, 1968. https://doi.org/10.1126/science.161.3837.186
22. Glasser MF, Coalson TS, Robinson EC, Hacker CD, Harwell J, Yacoub E, Ugurbil K, Andersson J, Beckmann CF, Jenkinson M, Smith SM, Van Essen DC: A multi-modal parcellation of human cerebral cortex. Nature 536:171-178, 2016. https://doi.org/10.1038/nature18933
23. Gong G, Jiang T, Zhu C, Zang Y, He Y, Xie S, Xiao J: Side and handedness effects on the cingulum from diffusion tensor imaging. Neuroreport 16:1701-1705, 2005. https://doi.org/10.1097/01.wnr.0000183327.98370.6a
24. Gonzalez-Romo NI, Hanalioglu S, Mignucci-Jiménez G, Abramov I, Xu Y, Preul MC: Anatomic depth estimation and 3-dimensional reconstruction of microsurgical anatomy using monoscopic high-definition photogrammetry and machine learning. Oper Neurosurg 24:432-444, 2023. https://doi.org/10.1227/ons.0000000000000544
25. Gurses ME, Gungor A, Gökalp E, Hanalioglu S, Karatas Okumus SY, Tatar I, Berker M, Cohen-Gadol AA, Türe U: Three-dimensional modeling and augmented and virtual reality simulations of the white matter anatomy of the cerebrum. Oper Neurosurg 23:355-366, 2022. https://doi.org/10.1227/ons.0000000000000361.
26. Gurses ME, Gungor A, Hanalioglu S, Yaltirik CK, Postuk HC, Berker M, Türe U: Qlone®: A simple method to create 360-degree photogrammetry-based 3-dimensional model of cadaveric specimens. Oper Neurosurg 21:E488-E493, 2021. https://doi.org/10.1093/ons/opab355.
27. Gurses ME, Gungor A, Rahmanov S, Gökalp E, Hanalioglu S, Berker M, Cohen-Gadol AA, Türe U: Three-dimensional modeling and augmented reality and virtual reality simulation of fiber dissection of the cerebellum and brainstem. Oper Neurosurg 23:345-354, 2022. https://doi.org/10.1227/ons.0000000000000358.
28. Gurses ME, Hanalioglu S, Mignucci-Jiménez G, Gökalp E, Gonzalez-Romo NI, Gungor A, Cohen-Gadol AA, Türe U, Lawton MT, Preul MC: Three-dimensional modeling and extended reality simulations of the cross-sectional anatomy of the cerebrum, cerebellum, and brainstem. Oper Neurosurg 25:3-10, 2023. https://doi.org/10.1227/ons.0000000000000703.
29. Gurses ME, Yangi K, Hanalioglu S, Akdemir Aktas H, Gok E, Tunc O, Lawton MT, Preul MC: Subtonsillar and vallecular triangles as gateways to dorsal brainstem and fourth ventricle lesions: descriptive and quantitative analysis of microsurgical anatomy. Neurosurg Rev 48:761, 2025. https://doi.org/10.1007/s10143-025-03876-5
30. Häberling IS, Badzakova-Trajkov G, Corballis MC: Asymmetries of the arcuate fasciculus in monozygotic twins: genetic and nongenetic influences. PLoS One 8:e52315, 2013. https://doi.org/10.1371/journal.pone.0052315
31. Hanalioglu S, Bahadir S, Isikay I, Celtikci P, Celtikci E, Yeh FC, Oguz KK, Khaniyev T: Group-level ranking-based hubness analysis of human brain connectome reveals significant interhemispheric asymmetry and intraparcel heterogeneities. Front Neurosci 15:782995, 2021. https://doi.org/10.3389/fnins.2021.782995.
32. Hanalioglu S, Bahadir S, Ozak AC, Yangi K, Mignucci-Jiménez G, Gurses ME, Fuentes A, Mathew E, Graham DT, Altug MY, Gok E, Turner GH, Lawton MT, Preul MC: Ultrahigh-resolution 7-Tesla anatomic magnetic resonance imaging and diffusion tensor imaging of ex vivo formalin-fixed human brainstem-cerebellum complex. Front Hum Neurosci 18:1484431, 2024. https://doi.org/10.3389/fnhum.2024.1484431
33. Hanalioglu S, Yangi K, Gurses ME, Aktas HA, Gok E, Tunc O, Lawton MT, Preul MC: Supracerebellar-supratrochlear and supracerebellar-infratrochlear triangles as gateways to the posterolateral midbrain and ambient cistern: descriptive and quantitative analysis of microsurgical anatomy. Neurosurg Rev 48:568, 2025. https://doi.org/10.1007/s10143-025-03688-7
34. Herbet G, Maheu M, Costi E, Lafargue G, Duffau H: Mapping neuroplastic potential in brain-damaged patients. Brain 139:829-844, 2016. https://doi.org/10.1093/brain/awv394
35. Herbet G, Zemmoura I, Duffau H: Functional anatomy of the inferior longitudinal fasciculus: from historical reports to current hypotheses. Front Neuroanat 12:77, 2018. https://doi.org/10.3389/fnana.2018.00077
36. Isikay AI, Gurses ME, Gecici NN, Baylarov B, Cekic E, Narin F, Karakaya D, Hanalioglu S, Bilginer B: Congenital brain tumors: surgical outcomes and long-term prognostic factors. World Neurosurg 191:e664-e673, 2024. https://doi.org/10.1016/j.wneu.2024.09.021.
37. Isikay I, Cekic E, Baylarov B, Tunc O, Hanalioglu S: Narrative review of patient-specific 3D visualization and reality technologies in skull base neurosurgery: enhancements in surgical training, planning, and navigation. Front Surg 11:1427844, 2024. https://doi.org/10.3389/fsurg.2024.1427844

38. Janelle F, Iorio-Morin C, D'amour S, Fortin D: Superior longitudinal fasciculus: a review of the anatomical descriptions with functional correlates. Front Neurol 13:794618, 2022. https://doi.org/10.3389/fneur.2022.794618
39. Jbabdi S, Johansen-Berg H. Tractography: where do we go from here? Brain Connect 1:169-183, 2011. https://doi.org/10.1089/brain.2011.0033
40. Jones DK, Christiansen KF, Chapman RJ, Aggleton JP: Distinct subdivisions of the cingulum bundle revealed by diffusion MRI fibre tracking: implications for neuropsychological investigations. Neuropsychologia 51(1):67-78, 2013. https://doi.org/10.1016/j.neuropsychologia.2012.11.018
41. Jun M, Shaobo S, Shuyuan Y, Yan Z, Yonggang L, Xiaochen C, Hui M: Preoperative visualization of cranial nerves in skull base tumor surgery using diffusion tensor imaging technology. Turk Neurosurg 26:805-812, 2016. https://doi.org/10.5137/1019-5149.JTN.13655-14.1
42. Khaniyev T, Cekic E, Gecici NN, Can S, Ata N, Ulgu MM, Birinci S, Isikay AI, Bakir A, Arat A, Hanalioglu S: Predicting mortality in subarachnoid hemorrhage patients using big data and machine learning: a nationwide study in Türkiye. J Clin Med 14:1144, 2025. https://doi.org/10.3390/jcm14041144
43. Khaniyev T, Cekic E, Koc MA, Dogan I, Hanalioglu S: Evaluating the machine learning models in predicting intensive care unit discharge for neurosurgical patients undergoing craniotomy: a big data analysis. Neurocrit Care 43:512-529, 2025. https://doi.org/10.1007/s12028-025-02246-9
44. La Corte E, Eldahaby D, Greco E, Aquino D, Bertolini G, Levi V, Ottenhausen M, Demichelis G, Romito LM, Acerbi F, Broggi M, Schiariti MP, Ferroli P, Bruzzone MG, Serrao G: The frontal aslant tract: a systematic review for neurosurgical applications. Front Neuro 12:641586, 2021. https://doi.org/10.3389/fneur.2021.641586
45. Makris N, Kennedy DN, McInerney S, Sorensen AG, Wang R, Caviness VS Jr, Pandya DN: Segmentation of subcomponents within the superior longitudinal fascicle in humans: a quantitative, in vivo, DT-MRI study. Cereb Cortex 15:854-869, 2005. https://doi.org/10.1093/cercor/bhh186
46. Martínez Santos JL, Aljuboori Z, Richardson AM, Hanalioglu S, Peker HO, Aydin I, Al-Sharshahi ZF, Tunc O, Karatas D, Avci E, Baskaya MK: Microsurgical anatomy and approaches to thalamic gliomas. Part 1: A cartography guide for navigating to the thalamus. Integrating 3D model rendering with anatomical dissections. J Neurosurg 141:1457-1471, 2024. https://doi.org/10.3171/2024.3.JNS232049
47. Martino J, De Witt Hamer PC, Berger MS, Lawton MT, Arnold CM, de Lucas EM, Duffau H: Analysis of the subcomponents and cortical terminations of the perisylvian superior longitudinal fasciculus: a fiber dissection and DTI tractography study. Brain Struct Funct 218:105-121, 2013. https://doi.org/10.1007/s00429-012-0386-5
48. Oldfield RC: The assessment and analysis of handedness: the Edinburgh inventory. Neuropsychologia 9:97-113, 1971. https://doi.org/10.1016/0028-3932(71)90067-4
49. Panesar SS, Belo JTA, Yeh FC, Fernandez-Miranda JC: Structure, asymmetry, and connectivity of the human temporo-parietal aslant and vertical occipital fasciculi. Brain Struct Funct 224:907-923, 2018. https://doi.org/10.1007/s00429-018-1812-0
50. Potgieser ARE, Wagemakers M, van Hulzen ALJ, de Jong BM, Hoving EW, Groen RJM: The role of diffusion tensor imaging in brain tumor surgery: A review of the literature. Clin Neurol Neurosurg 124:51-58, 2014. https://doi.org/10.1016/j.clineuro.2014.06.009
51. Powell HWR, Parker GJM, Alexander DC, Symms MR, Boulby PA, Wheeler-Kingshott CAM, Barker GJ, Noppeney U, Koepp MJ, Duncan JS: Hemispheric asymmetries in language-related pathways: a combined functional MRI and tractography study. Neuroimage 32:388-99, 2006. https://doi.org/10.1016/j.neuroimage.2006.03.011
52. Rheault F, De Benedictis A, Daducci A, Maffei C, Tax CMW, Romascano D, Caverzasi E, Morency FC, Corrivetti F, Pestilli F, Girard G, Theaud G, Zemmoura I, Hau J, Glavin K, Jordan KM, Pomiecko K, Chamberland M, Barakovic M, Goyette N, Poulin P, Chenot Q, Panesar SS, Sarubbo S, Petit L, Descoteaux M: Tractostorm: The what, why, and how of tractography dissection reproducibility. Hum Brain Mapp 41:1859-1874, 2020. https://doi.org/10.1002/hbm.24917
53. Shen CY, Tyan YS, Kuo LW, Wu CW, Weng JC: Quantitative evaluation of rabbit brain injury after cerebral hemisphere radiation exposure using generalized q-sampling imaging. PLOS ONE 10:e0133001, 2015. https://doi.org/10.1371/journal.pone.0133001
54. Song SK, Sun SW, Ju WK, Lin SJ, Cross AH, Neufeld AH: Diffusion tensor imaging detects and differentiates axon and myelin degeneration in mouse optic nerve after retinal ischemia. Neuroimage 20:1714-1722, 2003. https://doi.org/10.1016/j.neuroimage.2003.07.005
55. Song SK, Sun SW, Ramsbottom MJ, Chang C, Russell J, Cross AH: Dysmyelination revealed through mri as increased radial (but unchanged axial) diffusion of water. Neuroimage 17:1429-1436, 2002. https://doi.org/10.1006/nimg.2002.1267
56. Song SK, Yoshino J, Le TQ, Lin SJ, Sun SW, Cross AH, Armstrong RC: Demyelination increases radial diffusivity in corpus callosum of mouse brain. Neuroimage 26:132-140, 2005. https://doi.org/10.1016/j.neuroimage.2005.01.028
57. Thiebaut de Schotten M, Dell'Acqua F, Valabregue R, Catani M: Monkey to human comparative anatomy of the frontal lobe association tracts. Cortex 48:82-96, 2012. https://doi.org/10.1016/j.cortex.2011.10.001
58. Tomasi D, Volkow ND: Associations between handedness and brain functional connectivity patterns in children. Nat Commun 15:2355, 2024. https://doi.org/10.1038/s41467-024-46690-1
59. Vergani F, Ghimire P, Rajashekhar D, Dell'Acqua F, Lavrador JP: Superior longitudinal fasciculus (SLF) I and II: an anatomical and functional review. J Neurosurg Sci 65:560-565, 2021. https://doi.org/10.23736/S0390-5616.21.05327-3
60. Vernooij MW, Smits M, Wielopolski PA, Houston GC, Krestin GP, van der Lugt A: Fiber density asymmetry of the arcuate fasciculus in relation to functional hemispheric language lateralization in both right- and left-handed healthy subjects: A combined fmri and DTI study. Neuroimage 35:1064-1076, 2007. https://doi.org/10.1016/j.neuroimage.2006.12.041
61. Von Der Heide RJ, Skipper LM, Klobusicky E, Olson IR: Dissecting the uncinate fasciculus: disorders, controversies and a hypothesis. Brain 136:1692-1707, 2013. https://doi.org/10.1093/brain/awt094

62. Wu Y, Sun D, Wang Y, Wang Y, Ou S: Segmentation of the cingulum bundle in the human brain: a new perspective based on dsi tractography and fiber dissection study. Front Neuroanat 10:84, 2016. https://doi.org/10.3389/fnana.2016.00084
63. Yangi K, Gok E, Chen J, Demir Yangi D, Goyal M, Puppalla P, Kupanoff K, Li B, Koktekir E, Emmez OH, Preul M: A comparative study of large language models in turkish neurosurgery education using a mock neurosurgery board examination. Turk Neurosurg 36:183-199, 2026. https://doi.org/10.5137/1019-5149.JTN.50196-25.3
64. Yazbek S, Hage S, Mallak I, Smayra T: Tractography of the arcuate fasciculus in healthy right-handed and left-handed multilingual subjects and its relation to language lateralization on functional MRI. Sci Rep 11:20936, 2021. https://doi.org/10.1038/s41598-021-00490-5
65. Yeh FC, Irimia A, Bastos DCA, Golby AJ: Tractography methods and findings in brain tumors and traumatic brain injury. Neuroimage 245:118651, 2021. https://doi.org/10.1016/j.neuroimage.2021.118651
66. Yeh FC, Liu L, Hitchens TK, Wu YL: Mapping immune cell infiltration using restricted diffusion MRI. Magn Reson Med 77:603-612, 2017. https://doi.org/10.1002/mrm.26143
67. Yeh FC, Wedeen VJ, Tseng WY: Generalized q-sampling imaging. IEEE Trans Med Imaging 29:1626-1635, 2010. https://doi.org/10.1109/TMI.2010.2045126
68. Yeh FC, Zaydan IM, Suski VR, Lacomis D, Richardson RM, Maroon JC, Barrios-Martinez J: Differential tractography as a track-based biomarker for neuronal injury. Neuroimage 202:116131, 2019. https://doi.org/10.1016/j.neuroimage.2019.116131
69. Yuanzheng H, Lichao M, Xiaolei C, Bainan X: Functional outcome of surgery for glioma directly adjacent to pyramidal tract depicted by diffusion-tensor based fiber tracking. Turk Neurosurg 25:438-445, 2015. https://doi.org/10.5137/1019-5149.JTN.12001-14.1.
70. Yuzkan S, Karagulle M, Sam Ozdemir M, Mutlu S, Kocak B: Predictive value of T2-weighted perfusion and t1-weighted permeability MRI parameters in determining idh mutation status and grade of gliomas. Turk Neurosurg 34:1056-1065, 2024. https://doi.org/10.5137/1019-5149.JTN.46251-24.3
71. Zhang H, Schneider T, Wheeler-Kingshott CA, Alexander DC: NODDI: Practical in vivo neurite orientation dispersion and density imaging of the human brain. Neuroimage 61:1000-1016, 2012. https://doi.org/10.1016/j.neuroimage.2012.03.072